AFRL-AFOSR-JP-TR-2020-0026

Natural Materials Utilized Artificial Cork Synthesis

Jonghwan Suhr
Sungkyunkwan University Research & Business
2066 Seobu-ro, Jangan-gu
Suwon,, 16419
KR

10/26/2020
Final Report

Air Force Research Laboratory
Air Force Office of Scientific Research
Asian Office of Aerospace Research and Development
Unit 45002, APO AP 96338-5002

REPORT DOCUMENTATION PAGE

Form Approved
OMB No. 0704-0188

1. REPORT DATE *(DD-MM-YYYY)*	2. REPORT TYPE	3. DATES COVERED *(From - To)*
26-10-2020	Final	06 Aug 2018 to 05 Aug 2019

4. TITLE AND SUBTITLE
Natural Materials Utilized Artificial Cork Synthesis

5a. CONTRACT NUMBER

5b. GRANT NUMBER
FA2386-18-1-4035

5c. PROGRAM ELEMENT NUMBER
61102F

6. AUTHOR(S)
Jonghwan Suhr

5d. PROJECT NUMBER

5e. TASK NUMBER

5f. WORK UNIT NUMBER

7. PERFORMING ORGANIZATION NAME(S) AND ADDRESS(ES)
Sungkyunkwan University Research & Business
2066 Seobu-ro, Jangan-gu
Suwon,, 16419 KR

8. PERFORMING ORGANIZATION REPORT NUMBER

9. SPONSORING/MONITORING AGENCY NAME(S) AND ADDRESS(ES)
AOARD
UNIT 45002
APO AP 96338-5002

10. SPONSOR/MONITOR'S ACRONYM(S)
AFRL/AFOSR IOA

11. SPONSOR/MONITOR'S REPORT NUMBER(S)
AFRL-AFOSR-JP-TR-2020-0026

12. DISTRIBUTION/AVAILABILITY STATEMENT
A DISTRIBUTION UNLIMITED: PB Public Release

13. SUPPLEMENTARY NOTES

14. ABSTRACT
The depolymerized suberin derivatives (DSDs) were extracted from cork by environmentally-friendly alkaline hydrolysis. The stoichiometry control for the esterification of the DSDs was performed to determine an adequate amount of glycerol (5.87 wt%) by using 1H NMR. The expansion behavior of thermally expandable microspheres(TEMs) was characterized to form a closed-cell structure. Polyesterification of the DSDs and the expansion of TEMs were examined to synthesize the artificial cork (p-DSDs foam). The hysteresis energies of the p-DSDs foam and cork were 0.031 MJ/m3 and 0.012 MJ/m3, respectively, for 30% strain cyclic loading. This work could have a broad impact on enhancing the value of the recyclable natural materials and designing damping properties of the artificial cork foam material for various advanced applications, e.g., aerospace, automobile, and so on.

15. SUBJECT TERMS
natural cork, artificial cork, synthesis, closed-cell morphology

16. SECURITY CLASSIFICATION OF:			17. LIMITATION OF ABSTRACT	18. NUMBER OF PAGES	19a. NAME OF RESPONSIBLE PERSON
a. REPORT	b. ABSTRACT	c. THIS PAGE			KNOPP, JEREMY
Unclassified	Unclassified	Unclassified	SAR		19b. TELEPHONE NUMBER *(Include area code)* 315-227-7006

TABLE OF CONTENTS

Section Page

LIST OF FIGURES

Page

LIST OF TABLES

Page

1.0 SUMMARY

Cork is a natural and renewable material that exhibit intriguing material properties. However, due to its non-uniform material properties caused by its chemical composition and restricted distribution, cork has been used in limited applications although it shows outstanding damping and insulating properties. To resolve the challenges, in this work, artificial cork synthesis was studied. The depolymerized suberin derivatives (DSDs) were extracted from cork by environmentally-friendly alkaline hydrolysis. The stoichiometry control for the esterification of the DSDs was performed to determine an adequate amount of glycerol (5.87 wt%) by using ^{1}H NMR. The expansion behavior of thermally expandable microspheres(TEMs) was characterized to form a closed-cell structure. Polyesterification of the DSDs and the expansion of TEMs were examined to synthesize the artificial cork (p-DSDs foam). The hysteresis energies of the p-DSDs foam and cork were 0.031 MJ/m^3 and 0.012 MJ/m^3, respectively, for 30% strain cyclic loading. This work could have a broad impact on enhancing the value of the recyclable natural materials and designing damping properties of the artificial cork foam material for various advanced applications, e.g., aerospace, automobile, and so on.

2.0 INTRODUCTION

Cork is the outer bark of the cork oak tree (*Quercus suber* L.), which is a 100% natural and renewable material. Annually 201 kilotons of cork are produced worldwide and they are generally used as wine stopper and construction materials (i.e., insulation cork boards (ICBs) for thermal and sound/vibration insulations) [1-4]. Outstanding performances of cork come from its intrinsic material properties such as light-weight (0.12~0.2 g/cm^3), near-zero Poisson coefficient, elastic and highly deformable under compression without fracture, high damping, low electrical (2.9 x 10^{-14} S/m) and thermal (0.04 W/mK) conductivity [4]. However, there exist challenges in employing cork into advanced applications. Natural cork exhibits non-uniform material properties because the chemical compositions vary depending on the harvesting region and environment. Moreover, cork oak trees have a restricted distribution to the western Mediterranean basin, with the most dominant areas located in Portugal and Spain (above 60% of total) [1]. This restricted natural cork availability, both in quality and geography, limits natural cork used in advanced applications. Apart from the traditional uses of cork, a new approach to utilizing abundant cork resources has been risen driven by the foreseeable depletion of fossil fuel and the need for sustainable development [5-7]. This approach is becoming more important for recycling the cork and its valuable chemical components (suberin, lignin, and cellulose) because almost 40 wt% of cork byproducts are currently used as biomass or discarded during the manufacturing process [8-10]. These chemical components of cork can be extracted and separated to be used as a precursor to macromolecular materials, particularly employing long-chain aliphatic units of suberin. It includes the use of suberin monomers as offset ink additives [11], starting macromonomers for the preparation of polyurethane prepolymers [12-14], rigid polyurethane materials [15], polyester prepolymers [16,17], and rigid polyester films [18]. However, there are still challenges for employing outstanding properties of natural cork into advanced applications. Therefore, in this project, we have suggested a new idea that aims to synthesize artificial cork by reassembling the chemical components extracted from natural cork (Figure 1). Suberin in natural cork was selectively depolymerized by alkaline hydrolysis so that depolymerized suberin derivatives (DSDs) were obtained. DSDs were repolymerized by controlling stoichiometry as a binding matrix of the artificial cork as it was originally found in natural cork. The unique closed-cell structures of natural cork were mimicked and achieved by thermally expandable microspheres (TEMs). The

mechanical properties of the artificial cork were characterized, and the results showed higher damping property (250% increase)than that of cork.

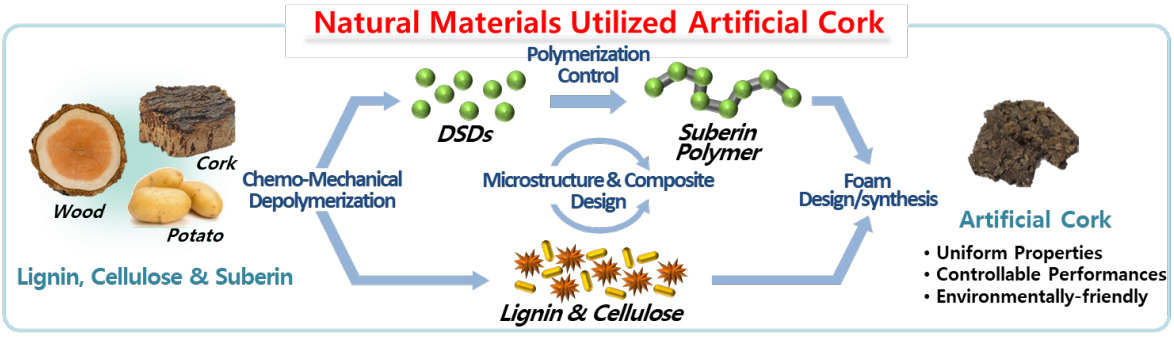

Figure 1. Schematic of natural materials utilized artificial cork

3.0 METHODS, ASSUMPTIONS, AND PROCEDURES

3.1 Materials

Expanded cork agglomerate was provided by Amorim (Portugal). Sodium hydroxide (NaOH, ≥98%), ethanol (≥99.7%), acetone (≥99%) and glycerol (≥99%) were purchased from Daejung Chemicals & Materials Co., Ltd (Korea). Trichloroacetyl isocyanate (TAI, 96%), Deuterochloroform ($CDCl_3$, ≥99.8%), 1,1,2,2-tetrachloroethane (TCE, ≥98%), N,O-Bis(trimethylsilyl)trifluoro acetamide with trimethylchlorosilane and sulfuric acid (95%) were purchased from Sigma-Aldrich (USA). Thermally expandable microspheres (CAP/264H) were provided by Kum Yang Co., Ltd (Korea).

3.2 Alkaline hydrolysis with grinding

20 g of expanded cork agglomerate and 4 g of sodium hydroxide were mixed with 500 ml of ethanol/water (4:1 v/v) solution. The mixture was poured into the blender and ground. During the grinding, the metal blade in the blender cut the expanded cork agglomerate into small-sized cork particles and stirred the mixture for the hydrolysis. The grinding was conducted for 1 h by grinding and cooling alternatively for 1 min to avoid overheating of the motor and boiling of the solution. After hydrolysis, the lignocellulosic residue was filtered with filter paper (pore size 7~9 μm). The dilute sulfuric acid was added to make the pH of the solution down to 3 and stirred for 1h at 70 °C. After cooling down at room temperature, the coagulated thick layer is gathered and washed with DI water 3 times at 70 °C temperature condition. The washed materials were freeze-dried and wax-like depolymerized suberin derivatives (DSDs) were obtained.

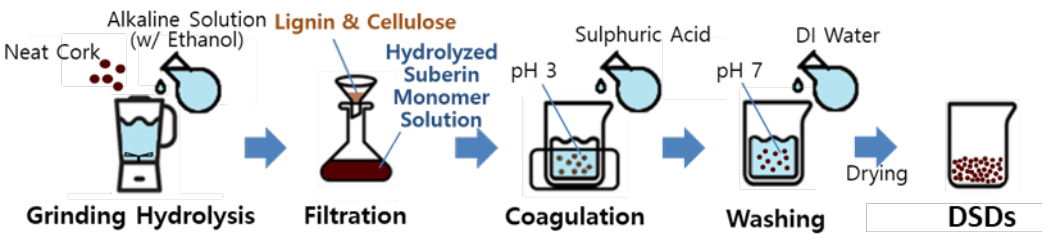

Figure 2. Alkaline hydrolysis of cork.

3.3 Bulk polyesterification of extracted cork suberin

Under 70 °C temperature conditions, 5.7 wt% of glycerol was added in the 7 g of DSDs to achieve the reaction stoichiometry between hydroxy and carboxylic acid groups. The mixture was stirred with a magnetic stirrer for 1 h. Then, the heated mixture was poured into the mold (5×5×4 cm) and heated in an oven (100 °C) for 72 h. During the heating, a vacuum was applied in the oven to remove the water generated during the esterification reaction. The resultant polymer is referred to as p-DSDs hereafter.

3.4 Preparation of suberin-based syntactic foams

5.7 wt% of glycerol and 20 wt% of TEMs were added in the 7 g of DSDs under 70 °C temperature condition. The mixture was stirred with a magnetic stirrer for 1 h. The mixture was poured into the mold (5×5×4 cm) and heated in the 150 °C vacuum oven for 3 min to expand the TEMs. Then, the TEMs expanded mixture was heated in a 100°C oven for 72 h. During heating, vacuum was applied in the oven to remove the water generated during the esterification reaction. The resultant syntactic foam is referred to as p-DSDs foam hereafter.

3.5 Characterization

Differential Scanning Calorimetry (DSC)

DSC thermograms were obtained with DSC Q20 (TA Instruments) using aluminum hermetic pans under constant purging nitrogen gas (50 ml/min). The analyses for suberin samples were performed between -50 and 200 °C. To analyze the expansion behavior of unbroken and broken thermally expandable microspheres were tested from -20 to 400 °C.

Thermogravimetric Analysis (TGA)

TGA was performed with TGA Q50 (TA Instruments) under a 50 ml/min nitrogen atmosphere. The temperature was heated up from 30 to 600 °C.

Gel Permeation Chromatography (GPC)

Molecular weights of the DSDs were analyzed by gel permeation chromatography (GPC) using the Agilent 1100S HPLC system (Agilent Technology). Tetrahydrofuran (THF) was used as the mobile phase with a flow of 1.0 ml/min. The DSDs-dissolved solutions (20.0 μl) were injected with 1.0 g/l of the DSDs concentration at 23 °C.

^{1}H NMR

In an NMR tube, 15 mg of DSDs which have a different weight fraction of glycerol was dissolved in 500 µl of $CDCl_3$. The mixtures were stirred to dissolve the DSDs completely. At room temperature, 50 µl of TAI was added in an argon atmosphere to avoid the reaction with moisture and to derivatize the –OH group in the DSDs and glycerol. ^1H NMR spectra were taken with Varian Oxford 300 MHz at 300.13 MHz with at least 64 scans.

Attenuated Total Reflection Fourier Transform Infrared Spectroscopy (ATR-FTIR)

FT-IR spectra were run with Bruker VERTEX 70v with an ATR add-on device. The tests were carried out at resolution 4 cm^{-1} with 50 scans.

Thermomechanical analysis (TMA)

Expansion behaviors of thermally expandable microspheres were analyzed by Seiko Exstar 6000 (Seiko Instrument). 10 mN pre-strain was applied by a probe to keep the contact between the sample and probe. The tests were carried out with isothermal mode for 120, 130, 140, and 150 °C temperature conditions. Until the temperature reaches the selected isothermal temperature, a temperature ramp rate with 10 °C/min was applied.

Scanning Electron Microscope (SEM)

SEM images were obtained by using a field emission scanning electron microscope (FE-SEM, JSM-7600F, JEOL) with an acceleration voltage of 10 kV. Before the analysis, Pt plasma was treated on the samples to coat and increase the electrical conductivity.

Monotonic Compression Test

Monotonic compression tests were carried out with the universal test machine by Electro Puls E-3000 (Instron). 12 mm diameter and 5 mm height cylindrical samples were prepared and placed between two flat platens. The tests were finished when the applied load reached to 80% compressive strain.

4.0 RESULTS AND DISCUSSION

4.1 Characterizations of DSDs

Figure 3 presents the ^1H NMR spectra of the DSDs extracted with alkaline hydrolysis, showing detailed chemical structures of the DSDs. The spectra showed an intense multiplet at $\delta \approx$ 1.25~1.31 ppm, attributed to CH_2 protons of the alkylic chains. A multiplet at $\delta \approx$ 1.61~1.71 ppm also comes from CH_2 protons, but in the β-position to the hydroxy ($–CH_2CH_2O–$) and ester ($–CH_2CH_2COO–$) groups. A multiplet at $\delta \approx$ 2.01 ppm is attributed to the allylic CH_2 protons adjacent to the unsaturated carbon (–CH=CH–) groups. A triplet at $\delta \approx$ 2.30~2.34 ppm corresponds to the resonances of the protons adjacent to the ester ($–CH_2COOCH_3$ or $–CH_2COOH$) groups. A multiplet at $\delta \approx$ 3.64~3.67 ppm is assigned to terminal $–CH_2OH$ protons overlapped with the resonances of mid-chain –CHOH proton resonance and protons adjacent

to the ester (–$COOCH_3$) groups. Lastly, a triplet at $\delta \approx 5.34$ ppm is attributed to the resonances of the protons of the unsaturated carbon (–CH=CH–) groups. The ^{1}H NMR spectra clearly indicate the presence of various carboxylic (~8%) and hydroxy (~2%) functional groups in the DSDs, determined by the relative quantitation of the signals (relative integral of the resonances). In addition, the concentration of unsaturated carbon groups was determined to be ~3% in the DSDs.

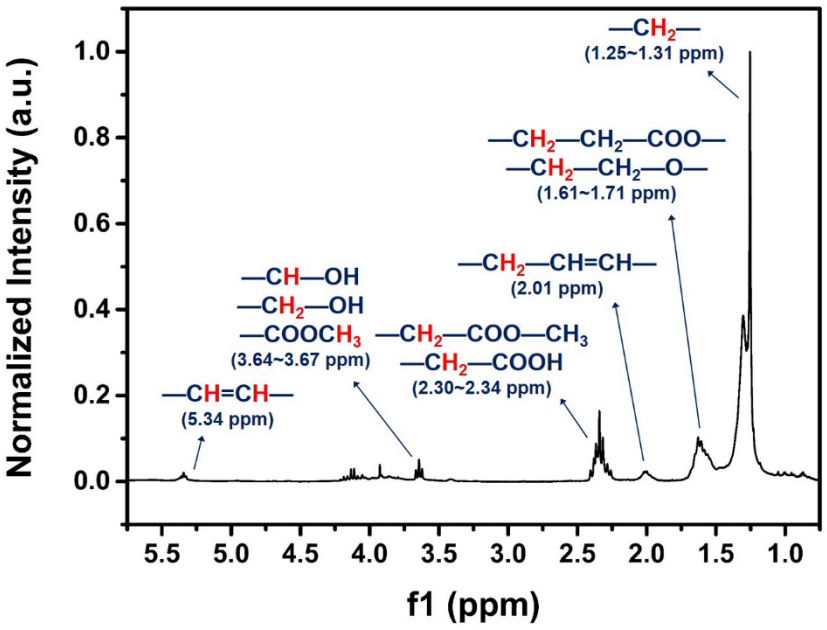

Figure 3. ^{1}H NMR spectra of DSDs

The molecular weight of DSDs was analyzed with GPC. The detected number-average molecular weight $\overline{M_n}$ and the weight-average molecular weight $\overline{M_w}$ was 780.74 and 1971.2 g/mol, respectively. This result revealed that the DSDs showed PDI (polydispersity index) of 2.52, indicating polydisperse molecular weight distributions of long hydrocarbon chains. By combining the results of ^{1}H NMR and GPC, the average number of hydrocarbons in the DSDs was estimated to be 22, which agrees with the references [4-5].

As shown in Figure 4a, the DSDs displayed a wide endothermic band from 25 °C to 66 °C. The melting temperature of the DSDs is observed to be 35 °C. However, to ensure its melted state, especially to mix with other materials, the temperature was needed to exceed 66 °C. The corresponding cooling curve exhibit an exothermic peak near 10 °C. This crystallization peak indicates that the DSDs have a low concentration of unsaturated carbon groups, which was confirmed from the ^{1}H NMR spectrum (~3%). The TGA thermograms are shown in Figure 4b. The DSDs were thermally stable up to approximately 250 °C (weight loss up to 3%). Above 250 °C, weight loss was significant due to the esterification, and evaporation of the water comes out during reaction. On the other hand, the weight loss of DSDs was not detected below 150 °C. If the material loss occurs, the ratio of hydroxy and carboxylic acid groups in DSDs can be

changed. Moreover, this change also affects the esterification reaction of DSDs. To keep the number of functional groups in DSDs, the polymerization needs to be conducted below 150 °C.

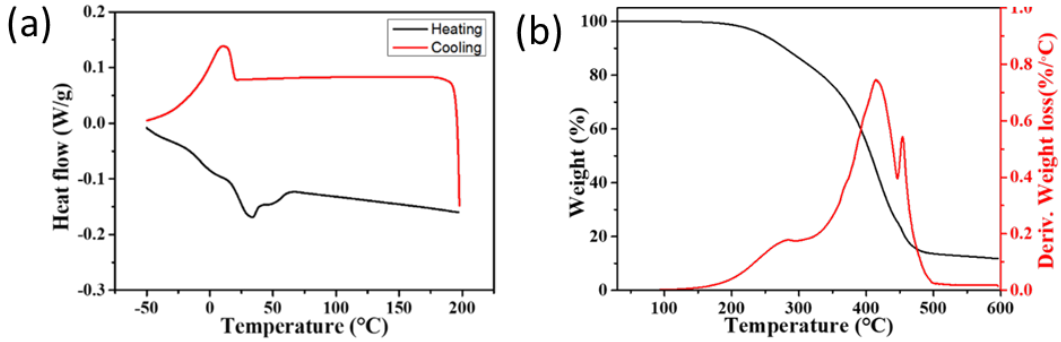

Figure 4. Thermal analysis results of DSDs: (a) DSC and (b) TGA.

4.2 Stoichiometry control for esterification of DSDs

Esterification between glycerol and carboxylic acid groups in the DSDs is a major reaction mechanism for repolymerizing the DSDs into polymeric materials. However, during the filtration process after grinding hydrolysis, most of the glycerols are dissolved in water [19]. Glycerol is a major crosslink agent in DSDs, which can participate in the esterification reaction of the DSDs [4, 5, 20, 21]. However, due to its loss, the stoichiometry of the hydroxy group and the carboxylic group in the DSDs is needed to be modified for better conversion and yield of the polymerization. The ^{1}H NMR analysis was applied to quantify the carboxylic acid and hydroxy group in the DSDs because of inaccurate end-point estimation with conventional titration approaches [22]. Figure 5 shows the ^{1}H NMR results of the pure DSDs and DSDs derivatized with TAI and glycerol mixture derivatized with TAI. The spectra of DSDs have –CH_2COOH resonance and –CHOH and –CH_2OH overlapped resonances at 2.33 and 3.63 ppm, respectively. Those resonances are related to the carboxylic acid and hydroxy group.

After TAI derivatization, the DSDs showed essentially the same resonances as their DSDs counterparts except for resonance related to the hydroxy and carboxylic acid groups. After TAI derivatization, –CH_2COOH resonance was separated into four new resonances (–CH_2COOH-TAI) at 2.27, 2.37, 2.56, and 2.86 ppm. Also, CHOH and CH2OH resonance at 3.63 ppm was separated into two new resonances at 4.25 ppm (–CH_2OH-TAI) and 5.07 ppm (–CHOH-TAI), respectively. When glycerol was added into the DSDs and derivatized, two new resonances related to the TAI derivatized CH_2 protons (–Gly-CH_2OH-TAI) and one new resonance related to the TAI derivatized CH proton (–Gly-CHOH-TAI) were appeared at 4.53, 4.63 and 5.47 ppm, respectively. In figure 5, the intensity of –Gly-CH_2OH-TAI and –Gly-CHOH-TAI were increased when the DSDs was increased from 0 to 0.5 wt%.

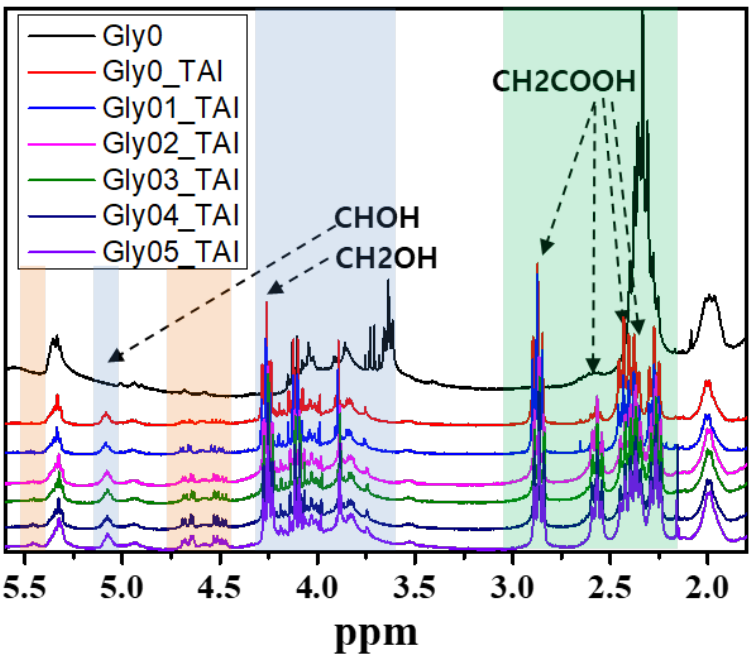

Figure 5. ^{1}H NMR spectra of DSDs before (Gly0) and after TAI derivatization with the addition of glycerol (Gly0_TAI, Gly01_TAI, Gly02_TAI, Gly03_TAI, Gly04_TAI, Gly05_TAI).

The ratio between the number of hydroxy and carboxylic acid groups (r) was determined with TAI derivatization by calculating the ratio between the integration area of –CH_2COOH-TAI for the carboxylic acid group and –Gly-CH_2OH-TAI, –CH_2OH-TAI, –Gly-CHOH-TAI, and –CHOH-TAI for the hydroxy group;

$$r = \frac{[A_{-CH2COOH-TAI}/2]}{[(A_{-Gly-CH2OH-TAI}+A_{-CH2OH-TAI})/2 \ +(A_{-Gly-CHOH-TAI}+A_{-CHOH-TAI})]} \quad (1)$$

The r-value of the DSDs without additional glycerol was calculated to be 2.74. This value indicates that the number of carboxylic acid groups in the DSDs is 2.74 times bigger than that of the hydroxy group. According to this calculation, the stoichiometry of the esterification reaction without further treatment will result in an incomplete reaction that will deteriorate the material properties. The low hydroxy group ratio comes from the glycerol loss during the filtration in the DSDs extraction process. The r values were fitted to the fractional function (y = 13.48701/(4.82417 + 1.5x)) for each DSDs mixture with respect to the amount of additional glycerol (Figure 6) to determine the adequate amount of glycerol to be added to the mixture for 1:1 stoichiometry of the hydroxy and carboxylic acid groups (r = 1). The R-square value of this equation was 0.97421. The expected glycerol amount to meet r = 1 was 5.87 wt%, and it was verified with the experimental result (r = 1.04).

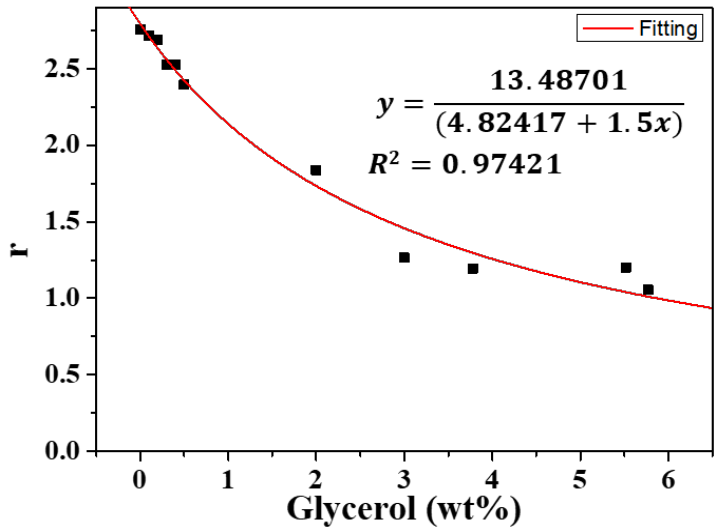

Figure 6. The ratio between the number of carboxylic and hydroxy groups.

Figure 7 shows FT-IR spectra of the DSDs and two different p-DSDs with or without additional glycerol (5.87 wt%). After polymerization of the DSDs through the esterification reaction, a new band around 1735 cm^{-1} that indicates C=O elongation of the ester group was observed. On the other hand, the band near 1703 cm^{-1}, attributed to the C=O carboxylic acid groups, was disappeared. The band detected around 3460 cm^{-1} which indicates the O-H hydroxy group was also absent in the FT-IR spectra of both p-DSDs. However, the band attributed to C=O carboxylic acid groups has remained in the spectra of p-DSDs without additional glycerol. All the hydroxy groups exist in the DSDs were not sufficient to make complete reaction with the carboxylic acid group in DSDs. This result agrees with the ^1H NMR analysis. On the other hand, the spectra of the p-DSDs with additional glycerol do not show C=O carboxylic acid group band. The hydroxy group in the added glycerol reacted with all the carboxylic acid groups and formed the ester bond during the esterification reaction.

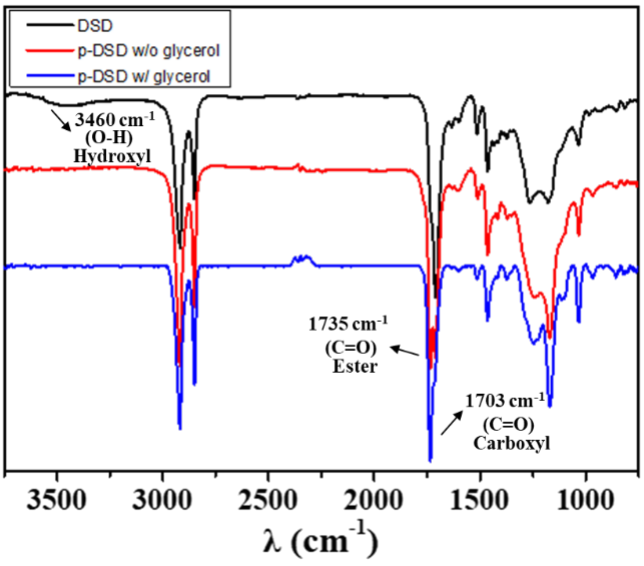

Figure 7. FT-IR spectra of DSDs, p-DSDs without additional glycerol, and p-DSDs with glycerol (5.87 wt%).

4.3 Characterization of thermally expandable microspheres (TEMs) for foaming

TEMs are hollow microspheres that have a polymeric shell and liquid hydrocarbon inside the shell. Thus, the microsphere expands its size when the heat is applied. To control the closed-cell microstructure with the expanded TEMs sizes, thermal characterization of the TEMs was conducted. Neat TEMs and the fractured TEMs (to remove liquid hydrocarbon inside the shell) were analyzed using DSC, and the results are shown in Figure 8a. It can be seen that the endothermic peak was detected at 117 °C. This peak appeared due to the vaporization of hydrocarbon liquid in the microspheres. The other small peaks were also detected at 126 and 140 °C, which may result from the inhomogeneous composition of the hydrocarbon liquid inside the microspheres. Figure 8b presents the DSC thermogram of the fractured TEMs to reveal the glass transition temperature (T_g) of the shell material. The T_g was observed at 83 °C and the shell of the TEMs become softer above the T_g. After the softening of its shell above 83 °C, the vaporized hydrocarbon increases inner pressure and it works as a driving force to expand the volume of the TEMs until the inner and outer pressure becomes equilibrium state.

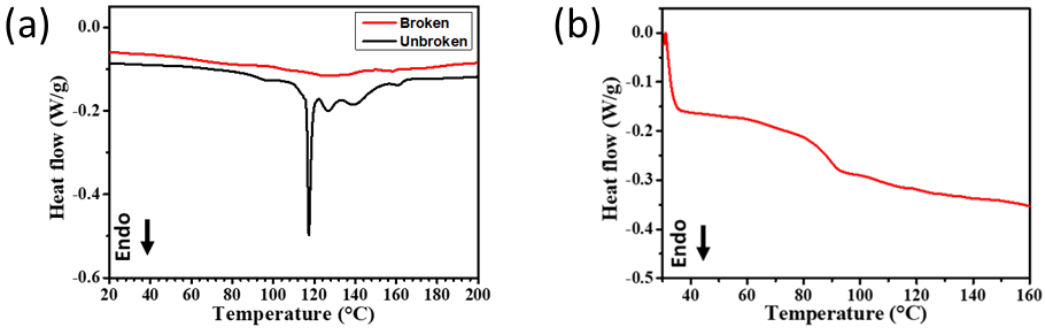

Figure 8. DSC analysis of TEMs: (a) DSC thermograms of broken and unbroken state TEMs and (b) DSC thermograms of broken state TEMs for determination of glass transition temperature.

In figure 9, the expansion behavior of the TEMs was analyzed by using TMA at an isothermal temperature from 110 to 150 °C. The dimension change is the sample thickness change to the initial thickness. The dimension change curve presents the expansion and shrinkage phase of the TEMs. The expansion rate was increased with temperature. The temperature accelerated the movement of vaporized hydrocarbon and it raised the inner pressure of the TEMs that drives the expansion [23, 24]. The rate of dimension change was gradually decreased when the pressure gap between the inner and outer microsphere decreased. At 140 and 150 °C, the dimension change was decreased after it reached the maximum value. It indicates the shrinkage of the TEMs, and the shrinkage became faster when the temperature was higher. As shown in figure 10, the shrinkage happens when the vaporized hydrocarbon dissipated through the cell wall that is thinned by expansion.

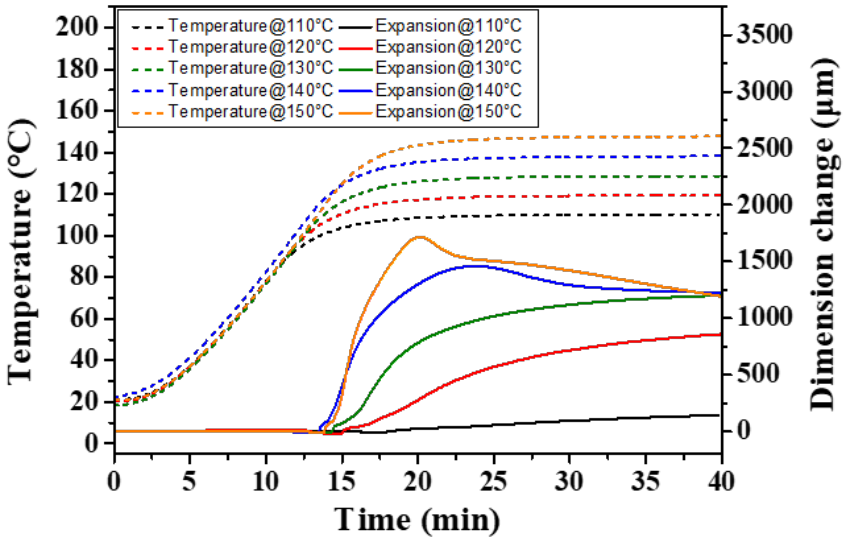

Figure 9. TMA of TEMs at various temperatures.

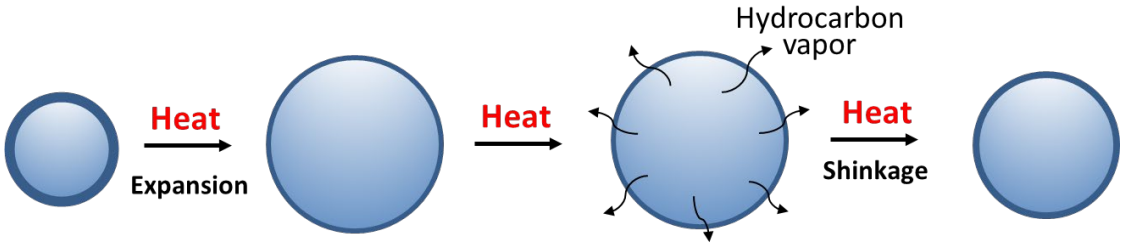

Figure 10. Shrinkage of TEMs by cell wall thinning

4.4 Characterization of p-DSDs foam

To synthesize the p-DSDs foam, different loading fraction of the TEMs were loaded in the DSDs. Figure 11 presents the cross-section of the p-DSDs foams. Before the expansion, the density of TEM is approximately 1.1 g/cm^3 [25]. However, when the TEMs are expanded, the density decreases, and they float in the melted state DSDs. As shown in figure 11, distinctive layers were observed where the TEMs only present on the top side of the composites below 15 wt% of TEMs loading fraction. The microstructure morphology of the p-DSDs foam (20 wt% of TEMs) and cork are shown in figure 12 with cell size and cell wall thickness comparison present in table 1. Both p-DSDs foam and cork exhibited a closed-cell structure. The p-DSDs foam showed deformed spherical shape cells because of the expansion of adjacent cells. Also, the cell walls of the p-DSDs foam were surrounded by the matrix (p-DSDs). On the other hand, natural cork showed relatively uniform rectangular shape close cells. Different from p-DSDs foam, cork cell walls were adjacent to each other. As shown in table 1, the average cell size of the p-DSDs was approximately 200% bigger than the average cell size of the cork cell. On the other hand, the cell wall thickness of the p-DSDs foam (1.8 μm) and cork (2 μm) exhibits similar cell wall thickness.

Figure 11. The cross section of p-DSDs foam: (a) 5 wt%, (b) 10 wt%, (c) 15wt%, (d) 20 wt%.

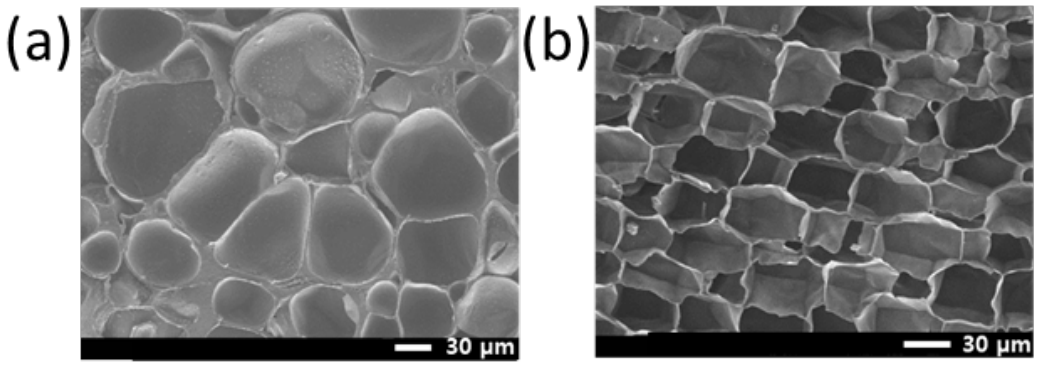

Figure 12. SEM images of (a) p-DSDs foam and (b) natural cork.

Table 1. The cell size and the cell wall thickness of cork and p-DSDs foam

	Cell size (µm)	Cell wall thickness (µm)
p-DSD foam	92	1.8
Cork	41	2

Figure 13 shows the uniaxial compression test results of the p-DSDs foam and natural cork. In the initial linear region, the p-DSDs and natural cork exhibited its compressive modulus as 1.37 and 1.42 MPa, respectively. This initial region is associated with the stiffness of cell walls in the p-DSDs foam and cork. This modulus might be decreased when the cell walls of the TEMs get thinner by the expansion. After the linear region, cell walls start to buckle in the plateau region. Finally, the densification region appeared when the upper and lower cell walls start to contact each other. The stress increment of the p-DSDs foam along with the compression strain was significant and it reached 11.3 MPa at 90% strain. On the other hand, cork showed 3 MPa at 90% strain. We assume this stress increment in the p-DSDs foam is due to the rigid unsaturated suberin polyester matrix. Different from the cork, p-DSDs foam is a composite that consists of the matrix (p-DSD) and the filler (TEMs). When the cells are compressed, the matrix affects the drastic increment of stress. The distinctive yield point was not observed after the linear region of the p-DSDs foam, whereas the syntactic foam with hollow glass microspheres shows the yield point [26]. It is possibly due to the softer cell walls of the TEMs while the glass microspheres are brittle. After the compression test, both p-DSD foam and cork were recovered to their original sample height. As shown in figure 14, the microstructure of the p-DSDs foam and cork kept its closed-cell structure without fracture due to its elasticity of the cell walls.

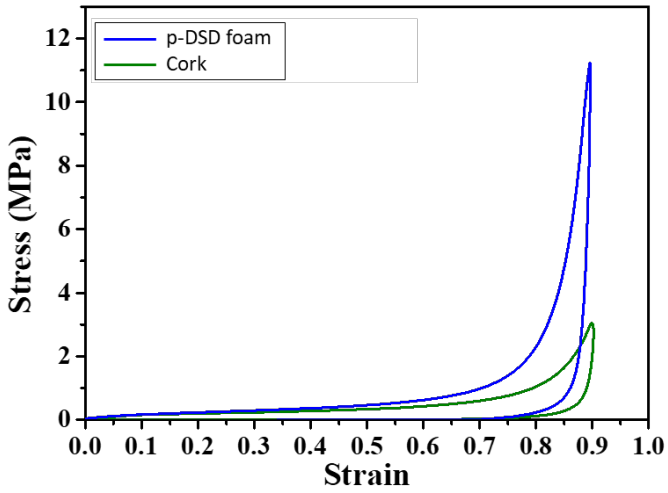

Figure 13. Uniaxial compression test results of p-DSDs foam and cork

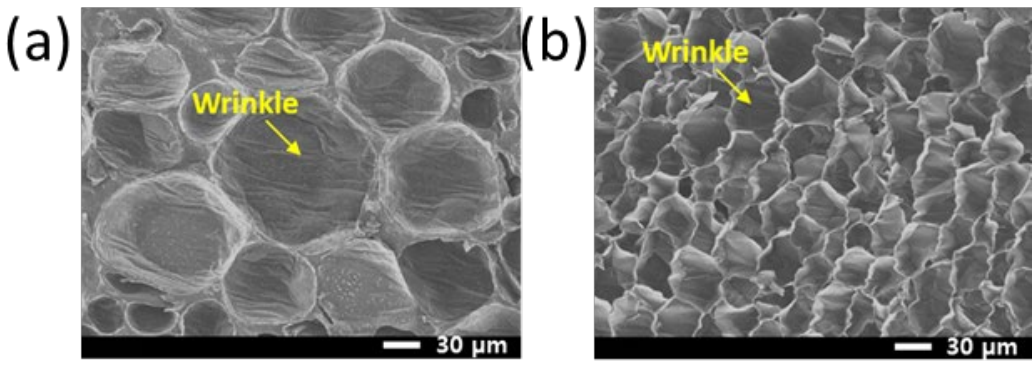

Figure 14. Microstructure morphology of compressed (a) p-DSDs foam and (b) cork

The loading and unloading curves for both p-DSDs foam and cork were compressed to 30% strain. As shown in figure 15, 10 cycles of compression tests were conducted. The samples were unloaded with the same strain rate as the loading strain rate. Both p-DSDs foam and cork did not return its original sample height after the first loading cycle and exhibited residual strain. This residual strain might attribute to the slow recovery of the cells. In figure 15, the p-DSDs and cork showed 5% deformation. This deformation might be caused by wrinkles formation due to the compressive load. The hysteresis energy of the p-DSDs foam and cork were 0.031 and 0.012 MJ/m^3, respectively. It indicates that p-DSDs foam absorbs approximately 250% more energy than cork. We assume the matrix and cell wall materials in the p-DSDs foam improve the energy absorption of the foams. During the loading, cell walls stand the load until they are buckled and the matrix increases the stress drastically when densification starts. On the other hand, stress was decreased rapidly by the elasticity of the matrix and cell walls during unloading.

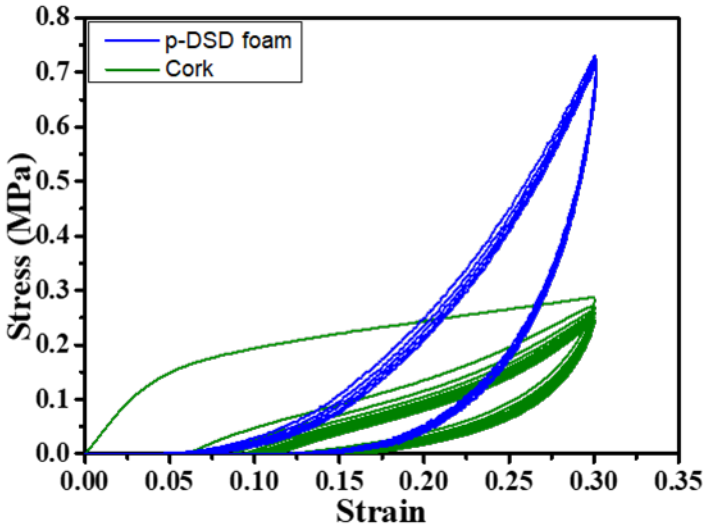

Figure 15. Cyclic test results of p-DSDs and cork

5.0 CONCLUSIONS

The newly developed artificial cork, namely p-DSDs foam, has been synthesized and its mechanical damping properties were characterized comparing with cork. The stoichiometry control for the esterification reaction has been presented by interpreting the hydroxy and carboxylic acid groups presented in the ^{1}H NMR spectra of DSDs. Also, the temperature conditions for the DSDs polymerization and TEMs expansion for cell morphology control were determined by the thermal analysis. In this study, we have successfully synthesized the p-DSDs foam with DSDs extracted from cork and have shown that the TEMs can form the closed-cell structure with the DSDs. The closed-cell morphology was observed for the synthesized p-DSDs foam. The mechanical test results showed superior damping properties (250% increase) of the p-DSDs foam than that of cork. With its higher damping properties, the p-DSDs foam has a potential impact on the application of damping material such as sandwich panel core materials, electrical vehicles, aircraft, and so on. Moreover, p-DSDs foam can reduce the carbon footprint by using cork byproducts for the extraction of the DSDs. With the more careful design of the cell size, cell wall thickness, and loading fraction of the TEMs, mechanical properties of the p-DSDs foam can be controlled for its specific applications. This work shows a promise to achieve a uniform and controllable properties of naturally derived materials as well as enhancing the value of the recyclable natural materials. Moreover, tunable damping capability of the artificial cork will provide an unprecedented opportunity to develop high performance and multifunctional composites for various advanced applications e.g. aerospace, automobile, and so on.

The results of this research were first introduced at the 2019 Fall Conference of the Korean Society for Composite Materials with the title of "A study on Suberin-based Polyester Syntactic Foam loaded with Thermally Expandable Microspheres".

The following three manuscripts related to this project are in preparation to submit in scientific journals: "Tunable Energy Absorbing Capabilities of Silica-filled Elastomer Composites by Engineering Filler–Filler and Filler–Matrix Interfaces with Nature-Derived Suberin Derivatives", "Environment-friendly Cork Suberin Derivatives based Artificial Cork with

High Damping Properties" and "Facile and environmentally-friendly approach for extraction of cellulose nanofibrils from natural materials". These results have the potential to integrate into various engineering research areas with its material-structure-property related characteristics and sustainable development for advanced applications (e.g., biopolymer composites, biodegradable polymer, bio-mimick materials, and so on).

6.0 REFERENCES

[1] APCOR *Yearbook*. 2015.

[2] Aroso, Ivo M., et al. "Cork: current technological developments and future perspectives for this natural, renewable, and sustainable material." *ACS Sustainable Chemistry & Engineering* 5.12 (2017): 11130-11146.

[3] Silva, S. P., et al. "Cork: properties, capabilities and applications." *International Materials Reviews* 50.6 (2005): 345-365.

[4] Pereira, Helena, ed. *Cork: biology, production and uses*. Elsevier, 2011.

[5] Gandini, Alessandro, Carlos Pascoal Neto, and Armando JD Silvestre. "Suberin: a promising renewable resource for novel macromolecular materials." *Progress in polymer science* 31.10 (2006): 878-892.

[6] Aroso, Ivo M., et al. "Cork: current technological developments and future perspectives for this natural, renewable, and sustainable material." *ACS Sustainable Chemistry & Engineering* 5.12 (2017): 11130-11146.

[7] Esteves, Bruno, et al. "Cork liquefaction for polyurethane foam production." *BioResources* 12.2 (2017): 2339-2353.

[8] Aroso, Ivo M., et al. "Cork: current technological developments and future perspectives for this natural, renewable, and sustainable material." *ACS Sustainable Chemistry & Engineering* 5.12 (2017): 11130-11146.

[9] Godinho, Maria Helena, et al. "Properties and processing of cork powder filled cellulose derivatives composites." *Macromolecular Symposia*. Vol. 169. No. 1. Weinheim: WILEY-VCH Verlag GmbH, 2001.

[10] Gerard, Jean-François, ed. *Fillers and filled polymers*. No. 169. John Wiley & Sons, 2001.

[11] Cordeiro, N., et al. "Cork suberin as an additive in offset lithographic printing inks." *Industrial Crops and Products* 11.1 (2000): 63-71.

[12] Garcia, Helga, et al. "Ex situ reconstitution of the plant biopolyester suberin as a film." *Biomacromolecules* 15.5 (2014): 1806-1813.

[13] Cordeiro, N., et al. "Urethanes and polyurethanes from suberin 2: synthesis and characterization." *Industrial Crops and Products* 10.1 (1999): 1-10.

[14] Evtiouguina, Margarita, et al. "Urethanes and polyurethanes based on oxypropylated cork: 1. Appraisal and reactivity of products." *Polymer international* 50.10 (2001): 1150-1155.

[15] Gama, Nuno V., et al. "Bio-based polyurethane foams toward applications beyond thermal

insulation." *Materials & Design* 76 (2015): 77-85.

[16] Sousa, Andreia F., et al. "Novel suberin-based biopolyesters: From synthesis to properties." *Journal of Polymer Science Part A: Polymer Chemistry* 49.10 (2011): 2281-2291.

[17] Sousa, Andreia F., et al. "Synthesis and characterization of novel biopolyesters from suberin and model comonomers." *ChemSusChem* 1.12 (2008): 1020-1025.

[18] Cordeiro, Nereida, et al. "Urethanes and polyurethanes from suberin: 1. Kinetic study." *Industrial Crops and Products* 6.2 (1997): 163-167.

[19] Ferreira, Rui, et al. "Unveiling the dual role of the cholinium hexanoate ionic liquid as solvent and catalyst in suberin depolymerisation." *RSC Advances* 4.6 (2014): 2993-3002.

[20] Deshmukh, Ashish P., et al. "Insights into the structure of cutin and cutan from Agave americana leaf cuticle using HRMAS NMR spectroscopy." *Organic Geochemistry* 36.7 (2005): 1072-1085.

[21] Pereira, Helena. "Variability of the chemical composition of cork." *BioResources* 8.2 (2013): 2246-2256.

[22] Sousa, Andreia F., et al. "Determination of the Hydroxy and Carboxylic Acid Groups in Natural Complex Mixtures of Hydroxy Fatty Acids by 1 H Nuclear Magnetic Resonance Spectroscopy." *Applied spectroscopy* 63.8 (2009): 873-878.

[23] Najib, N. N., et al. "Correlation between the acoustic and dynamic mechanical properties of natural rubber foam: Effect of foaming temperature." *Materials & Design* 32.2 (2011): 505-511.

[24] Wang, Lijun, et al. "The compressive properties of expandable microspheres/epoxy foams." *Composites Part B: Engineering* 56 (2014): 724-732.

[25] Ina, Maria, et al. "The design of wrinkled microcapsules for enhancement of release rate." *Journal of colloid and interface science* 478 (2016): 296-302.

[26] Yousaf, Zeshan, et al. "Compression properties of polymeric syntactic foam composites under cyclic loading." *Composites Part B: Engineering* 186 (2020): 107764